Research Article

Azhar U. Khan, Azmat Ali Khan, Nazia Malik, Jun Her, Mona Gupta, Subhranshu Panda, Khalid Imtiyaz, Mohammed Moshahid Alam Rizvi, Mohammed Mushtaque, Sudhakar M. Bansod, Masita Mohammad, Min Kim, Kyungsoo Pyo*, and Mahboob Alam*

Synthesis of Cu_4O_3 nanoparticles using pumpkin seed extract: Optimization, antimicrobial, and cytotoxicity studies

https://doi.org/10.1515/ntrev-2025-0203
received February 14, 2025; accepted July 1, 2025

Abstract: In pursuit of sustainable nanomaterials, this study presents a green synthesis approach for producing copper oxide (Cu_4O_3) nanoparticles (NPs) using pumpkin seed extract, a plant-based resource rich in bioactive compounds. Unlike conventional chemical methods, this eco-friendly route enables rapid, cost-effective NP production with minimal environmental impact. Notably, pumpkin seed extract serves a dual function as both a reducing and stabilizing agent during NP formation. The synthesized Cu_4O_3 NPs were comprehensively characterized using X-ray diffraction, thermogravimetric analysis, transmission electron microscopy, scanning electron microscopy with energy-dispersive X-ray spectroscopy (EDS), and UV–visible spectrophotometry. The NPs displayed sizes ranging from 8.92 to 55.84 nm, and the UV–Vis spectrum exhibited a characteristic peak at 332 nm, confirming Cu_4O_3 formation. A maximum predicted yield of 89.87% was achieved under optimized conditions (7.0 mM $CuSO_4$, 16.26 mL pumpkin seed extract, and 105.71°C), as determined using a Box–Behnken design. Furthermore, the biogenic Cu_4O_3 NPs demonstrated significant antibacterial activity against *Bacillus subtilis*, with an inhibition zone diameter of 2.8 cm at a concentration of 4 ppm, and moderate cytotoxic effects against A549 (lung adenocarcinoma) and HCT-116 (colon cancer) cell lines, as shown by MTT assays. Computational studies employing density functional theory elucidated the electronic structure and reactivity of the synthesized Cu_4O_3 NPs, revealing a moderate HOMO–LUMO energy gap (1.23 eV), indicative of potential interactions with biological systems, which may contribute to their observed antimicrobial and cytotoxic activities. These findings underscore the potential biomedical applications of pumpkin seed-mediated Cu_4O_3 NPs and provide a foundation for future research in green nanotechnology.

Keywords: biogenic approach, Cu_4O_3 nanoparticles, Box–Behnken design, cytotoxicity, antibacterial activity

*** Corresponding author: Kyungsoo Pyo**, Disaster Information Research Division, National Disaster Management Research Institute, Ulsan, 44538, Republic of Korea, e-mail: kspyo@korea.kr
*** Corresponding author: Mahboob Alam**, Department of Safety Engineering, Dongguk University WISE, 123, Dongdaero, Gyeongju-si, 38066, Republic of Korea, e-mail: mahboobchem@gmail.com
Azhar U. Khan: School of Life and Basic Sciences, Jaipur National University, Jaipur, India
Azmat Ali Khan: Pharmaceutical Biotechnology Laboratory, Department of Pharmaceutical Chemistry, College of Pharmacy, King Saud University, Riyadh, 11451, Saudi Arabia
Nazia Malik: Deaprtment of Chemistry, Aligarh Muslim University, Aligarh, 202002, India
Jun Her, **Min Kim:** Department of Safety Engineering, Dongguk University WISE, 123, Dongdaero, Gyeongju-si, 38066, Republic of Korea
Mona Gupta: Department of Physics, Govt. Holkar Science College, Devi Ahilya University, Indore, India
Subhranshu Panda: School of Pharmaceutical Sciences, Jaipur National University, Jaipur, India
Khalid Imtiyaz, **Mohammed Moshahid Alam Rizvi:** Department of Biosciences, Jamia Millia Islamia, New Delhi, 110025, India
Mohammed Mushtaque: Department of Chemistry, Marwari College (A constituent Unit of L.N. Mithila University, Kameshwarnagar), Darbhanga, Bihar, India
Sudhakar M. Bansod: BDRM, CSIR-Indian Institute of Chemical Technology, Hyderabad, 500007, Telangana, India
Masita Mohammad: Solar Energy Research Institute (SERI), Universiti Kebangsaan Malaysia, 43600 UKM Bangi, Selangor, Malaysia

1 Introduction

Nanotechnology is a rapidly growing field impacting various areas of modern science, including biotechnology and biomedical science. Nanomaterials, defined by having at least one dimension at the nanoscale [1], exhibit unique physicochemical properties such as enhanced charge storage, magnetic behavior, conductivity, and surface area, leading to improved performance compared to their bulk

counterparts in medicine, engineering, agriculture, and industry [2–4]. Nanoparticles (NPs), characterized by their shape, size, and distribution, can be synthesized through various methods, including electrochemical, microwave-assisted, and green synthesis approaches [5]. Their nanoscale dimensions enable them to interact with biological systems at the cellular level, facilitating applications in disease detection and drug delivery [6,7]. While organic NPs based on polymers, carbohydrates, lipids, nucleic acids, and proteins are generally considered non-toxic and biocompatible [8], inorganic NPs like ZnO, Cu, Au, and Ag are used in medicine and surface coatings to enhance stability and biocompatibility [8–11]. For example, ferumoxytol (iron NP) is used to treat anemia [12,13], and gold NPs exhibit optical properties used in diagnostics for detecting substances like ochratoxin A [14]. Organometallic NPs are also being explored for targeted drug delivery in diseases like cancer [15]. The use of biological materials such as plant extracts (leaves, flowers, fruit peel, seeds, stem bark), algae, fungi, and bacteria for NP fabrication offers a safe, reliable, less toxic, and eco-friendly approach with a wide range of applications [3,16–24]. Copper (Cu) is an essential element for plant growth and exhibits significant pharmacological properties, including antimicrobial, analgesic, anticancer, and anti-inflammatory effects [25,26]. Biologically, it acts as a crucial trace element and a cofactor for various enzymes [27,28], and it shows promise in targeted cancer therapies [29,30]. Copper can form different oxides, including CuO, Cu_2O, and the less common Cu_4O_3 (paramelaconite). While CuO and Cu_2O have applications in catalysis and energy conversion, Cu_4O_3, a mixed-valence copper oxide found in hydrothermal deposits, has shown potential in biological applications due to its unique properties [31,32]. Copper deficiency in plants can lead to various growth abnormalities [33,34].

In recent years, other NPs synthesized through plant-mediated green approaches have garnered significant interest due to their simplicity, eco-friendliness, and compatibility with biological systems. For example, silver NPs prepared using *Justica wynaadensis* leaf extract showed promising antibacterial, anticancer, antidiabetic, and anti-inflammatory properties [35]. Bimetallic ZnO–CuO NPs synthesized using *Aegle marmelos* extract demonstrated enhanced photocatalytic activity, attributed to the formation of p–n heterojunctions [36]. Likewise, Fe–Pd bimetallic NPs derived from *Ulmus davidiana* bark extract exhibited improved catalytic performance [37]. Recent research highlights the nutraceutical and therapeutic importance of nuts and seeds due to their bioactive constituents [38–42]. Pumpkin seeds, from the Cucurbitaceae family (*e.g.*, *Cucurbita pepo*, *C. moschata*, *C. maxima*) [43,44], are recognized as nutrient powerhouses with high nutraceutical potential [43–46]. They are utilized in various cultures for their ethnomedical benefits and as food additives [43–47]. Pumpkin seeds are rich in vitamin E, carotenoids, provitamins [47], pigments, squalene, pyrazines, saponins [48], phytosterols, phenolic compounds, triterpenoids [43,44,46,47], unsaturated fatty acids, flavonoids, proteins, and coumarins [49,50]. They also contain essential minerals like potassium, phosphorus, magnesium, copper, iron, and zinc [50,51]. These bioactive compounds and minerals contribute to various physiological benefits, including potential in preventing tumors [38,47,50], microbial infections [52–54], hyperglycemia [55], and prostate disorders [56–59]. Pumpkin seed extract also exhibits wound healing, hair growth stimulation, anthelmintic, hepatoprotective, antioxidant, and chemoprotective properties [41,44,54,60–66]. Taking advantage of this wealth of natural resources, the outer peels of two Ipomoea batatas varieties – Korean red skin and Korean pumpkin sweet potato, both rich in beneficial nutrients and bioactive compounds [67] served as a sustainable resource for synthesizing silver NPs. These biosynthesized NPs demonstrated promising bio-potential in antidiabetic, antioxidant, antibacterial, and cytotoxicity assays. A previous study reported the antibacterial and cytotoxic potential of Cu_4O_3 NPs synthesized using *Razma* seed extract [68].

Although plant-based synthesis of copper oxide NPs has been previously reported, the use of pumpkin seed extract for the green synthesis of Cu_4O_3 NPs remains largely unexplored. The rich phytochemical profile of pumpkin seeds, including phenolic compounds, flavonoids, and unsaturated fatty acids, provides a unique combination of reducing and stabilizing agents that may enhance the biological properties of the NPs. In particular, this study demonstrates that biosynthesized Cu_4O_3 NPs exhibit notable antibacterial and cytotoxic activities, suggesting that the synergistic effects between the Cu_4O_3 core and surface-bound bioactive molecules could be responsible for the enhanced bioactivity observed compared to earlier reports. Additionally, a molecular index analysis based on density functional theory (DFT) calculations was performed to further support the observed biological activities, revealing moderate chemical reactivity and favorable electronic properties for interactions with bacterial and cancer cells.

In this work, we explore the green synthesis of Cu_4O_3 NPs using pumpkin seed extract as a precursor. To optimize the synthesis process, we employed the Box–Behnken design (BBD), a response surface methodology (RSM) that minimizes the number of experimental runs while evaluating the interactions between variables to achieve maximum yield [69–72]. Furthermore, we characterized the

synthesized NPs using various spectroscopic and microscopic techniques and assessed their antibacterial and cytotoxic potential. Process parameters influencing NP productivity were also optimized to enhance both yield and biological efficacy.

2 Materials and methods

2.1 Materials

Pumpkin seeds were purchased near the JNU Market (Jaipur, Rajasthan, India). Copper sulfate was acquired from Merck and Sigma-Aldrich (India).

2.2 Preparation of pumpkin seed extract

The collected seeds were properly washed and dried. The dried seeds were then ground into fine powder using a suitable grinder. Subsequently, 150 mL of double-distilled water was added to 10 g of crushed seed powder in a 250 mL round-bottom flask. The solution was refluxed for 45 min. After cooling to room temperature, the extract was filtered using Whatman No. 1 filter paper for further processing.

2.3 Biogenic synthesis of Cu_4O_3 NPs

Copper oxide nanoparticles (Cu_4O_3 NPs) were produced using pumpkin seed extract by biomimetic synthesis. At room temperature, 20 mL of pumpkin seed extract was added to 90 mL of a 5 mM copper sulfate ($CuSO_4$) solution. To ensure proper mixing, the mixture was continually swirled for 20 min with a magnetic stirrer. The mixture was then refluxed at 97°C for 8 h, stirring constantly throughout. After reflux, the reaction mixture was allowed to come down to room temperature for 30–45 min. Finally, the mixture was dried in a hot air oven set to 60–90°C for 24 h before being stored in a sealed glass bottle (Scheme 1). To optimize the yield of NPs using the BBD, we carried out additional experiments focusing on three key factors: the concentration of $CuSO_4$ (in mM), the reaction temperature (in °C), and the volume of plant extract (in mL). For each type of plant extract, we prepared 15 conical flasks, labeled from 1 to 15. The yield of Cu_4O_3 NPs was then calculated by measuring the absorbance at a wavelength of 332 nm.

2.4 Characterization of biogenic Cu_4O_3 NPs

The synthesis of Cu_4O_3 NPs was verified using various physicochemical characterization techniques. UV–visible spectroscopy analysis was performed using a UV–Vis spectrophotometer (UV-1800, Shimadzu, Japan) to obtain the absorption spectra. Fourier-transform infrared (FTIR) spectroscopy was carried out using a Bruker Alpha FTIR spectrometer (Bruker Optik GmbH, Germany) to identify the functional groups based on the characteristic stretching frequencies in the range of 4,000–400 cm^{-1}. The KBr pellet method was used for sample preparation. FTIR spectroscopy was utilized to identify the functional groups in the bioactive constituents that contributed to the reduction, capping, and stabilization of Cu_4O_3 NPs synthesized using pumpkin seed extract.

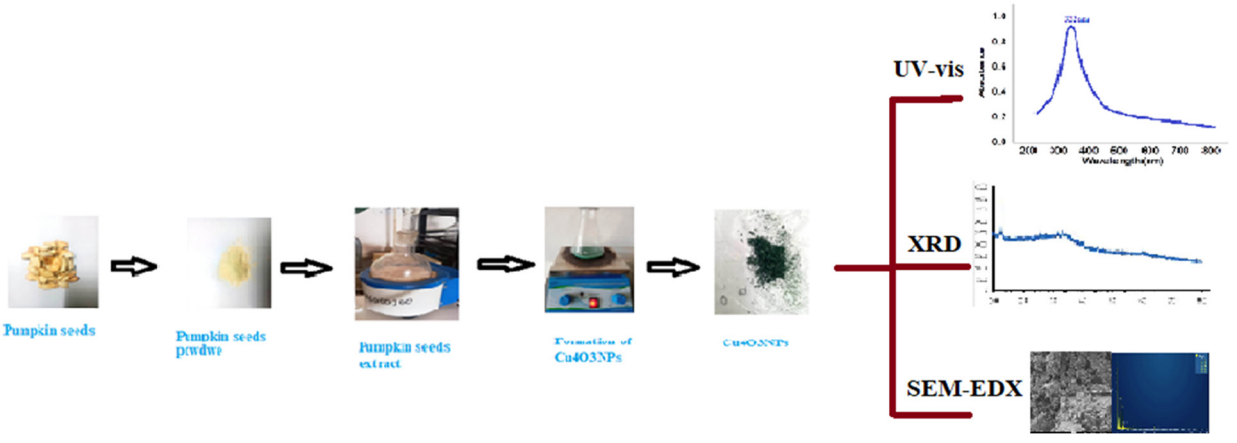

Scheme 1: Formation of Cu_4O_3 NPs from pumpkin seed extract.

To determine phase purity and the crystallite size, X-ray diffraction (XRD) analysis was conducted using a PANalytical X'Pert PRO diffractometer (Malvern Panalytical, Netherlands) with Cu Kα radiation (λ = 1.54 Å). The diffraction peaks were matched against standard JCPDS reference patterns. The XRD profile exhibited sharp peaks, confirming the crystalline nature of the NPs. Thermogravimetric analysis (TGA) was performed on a TGA 8000 (PerkinElmer, USA) instrument to assess thermal stability. A 2 mg sample was heated from 30 to 600°C at a rate of 10°C min^{-1} under a nitrogen atmosphere.

The morphology and elemental composition of the NPs were analyzed using a field-emission scanning electron microscope (FE-SEM; Nova NanoSEM 450, FEI, USA) equipped with energy-dispersive X-ray spectroscopy (EDX). High-resolution transmission electron microscopy (HR-TEM) was performed using a JEOL JEM-2100 (JEOL Ltd., Japan), operated at an accelerating voltage of 200 kV. The samples were drop-cast on carbon-coated copper grids for analysis.

2.5 Experimental design and data analysis

The BBD, a well-established statistical experimental design within the framework of RSM [73], was utilized to evaluate the effects of three key input variables – $CuSO_4$ concentration (mM), reaction temperature (°C), and extract volume (mL) – on the yield (%) of Cu_4O_3 NPs. BBD was selected for its efficiency and cost-effectiveness, requiring only 15 experimental runs to systematically explore the interactions between the variables. The experimental data were analyzed and fitted into a second-order polynomial equation model using Minitab software (Minitab® LLC, Pennsylvania, USA; Version 22.2.2.0, Academic Free Trial) [74], enabling the assessment of both individual and interactive effects of the variables on the NP yield. The BBD is known for its unique arrangement of experimental points, with three levels assigned to each factor, coded as −1, 0, and +1. This design is particularly advantageous for multiple regression analysis because it allows for efficient exploration of complex interactions using a minimal number of experiments. The model is well suited to approximating quadratic relationships and provides reliable coefficient estimates near the center of the experimental space. However, it is important to note that the precision of these estimates may decrease in the corners of the experimental domain, where there are no design points. Table 1 outlines the factors and levels employed in the BBD for optimizing Cu_4O_3 NP biosynthesis. This design aids in determining optimal conditions for maximizing NP yield and elucidates the interactions between variables, thereby improving the efficiency of NP synthesis.

Table 1: Factors and levels selected for BBD optimization of Cu_4O_3 NP biosynthesis

S. no.	Factors	Coded variable level		
		Low (−1)	Medium (0)	High (+1)
1	Concentration of $CuSO_4$ solution (mM)	3.0	5.0	7.0
2	Volume of pumpkin seed extract (mL)	10.0	20.0	30.0
3	Reaction temperature (°C)	85	97	110

2.6 Cytotoxicity study

2.6.1 Cell culture

The National Center for Cell Sciences in Pune, India, supplied the A549 lung cancer cell line and the HCT-116 colon cancer cell line. The cells were cultivated in Dulbecco's modified Eagle medium with the addition of 10% fetal calf serum, 100 units/mL penicillin, 100 g/mL streptomycin, and 2.5 g/mL amphotericin B. The temperature, relative humidity, and CO_2 levels were kept constant at 37°C, 80% relative humidity, and 5% CO_2, respectively.

2.6.2 MTT assay

An MTT assay was used to determine whether the NPs were cytotoxic to HCT-116 and A549 cancer cell lines. Among the most commonly used methods for assessing *in vitro* cytotoxicity, this assay employs 3,4,5-dimethylthiazol-2-yl-2,5-diphenyltetrazolium bromide (M2128 Sigma Aldrich) [75]. In summary, 96-well plates were filled with 1×10^4 cells per well (150 µL per well) and incubated overnight. After being incubated, the cells were subjected to different doses of NPs for a duration of 24 h. Following the treatment, the culture medium was extracted, and 20 µL of MTT solution (5 mg/mL in phosphate-buffered saline) was introduced into each well. The cells were subsequently placed in an incubator for a duration of 4 h to facilitate the reduction of the MTT dye by live cells, resulting in the formation of formazan crystals. Afterward, the formazan crystals were dissolved using 150 µL of DMSO in each well. Ultimately, the absorbance of the resultant solution was quantified at a wavelength of 570 nm using a plate reader (i-Mark, BIORAD, S/N 10321). Cell vitality, expressed as a percentage, was assessed by calculating the ratio of absorbance in treated cells to that in untreated controls.

2.7 Antibacterial activity

The antimicrobial efficacy of Cu_4O_3 nanoparticles (Cu_4O_3NPs) produced through biofabrication was assessed against a strain of *Bacillus subtilis* using the disc diffusion method. The bacterial inoculum was standardized to approximately 1×10^6 CFU/mL using the 0.5 McFarland standard. Nutrient agar plates were prepared, sterilized, and allowed to solidify. Following solidification, the bacterial culture was uniformly swabbed onto the plates. Cu_4O_3NPs were introduced into agar wells at concentrations ranging from 1 to 4 ppm. A control using only solvent (water) was also included. The plates were incubated at 37°C for 24 h without disturbance. After incubation, the diameters of the zones of inhibition were measured using digital calipers. The results were recorded as mean values from three independent replicates. Furthermore, the dimensions, morphology, and surface characteristics of Cu_4O_3NPs were also analyzed to understand their influence on antimicrobial activity.

2.8 Molecular index study

The geometry optimization of the Cu_4O_3 cluster was carried out using DFT as implemented in the Gaussian program [76]. The hybrid RB3LYP functional was employed, known for its good performance with transition metal oxides. A GenECP basis set (specifically, LANL2DZ for Cu to account for relativistic effects and 6-31G(d) for O) was used. The optimization was performed without any symmetry constraints, and the spin multiplicity was set to singlet ($S = 0$). The final optimized structure exhibited no imaginary frequencies, confirming that a true minimum was obtained. The convergence criteria were satisfied with a very small RMS gradient norm of 0.000011 a.u., and the total electronic energy at the optimized geometry was found to be −1009.95358203 atomic units. The Cu_4O_3 cluster optimized in the D_4h point group was then utilized for frontier molecular orbital (HOMO–LUMO) analysis and the calculation of global reactivity descriptors, including electronegativity, chemical hardness, and chemical softness, to provide insights into its potential biological interactions.

2.9 Statistical design and data processing

The experimental design and statistical analysis were conducted using Minitab® Statistical Software (Minitab LLC, Pennsylvania, USA; Version 22.2.2.0, Academic Free Trial) [74]. A full quadratic regression model was used to

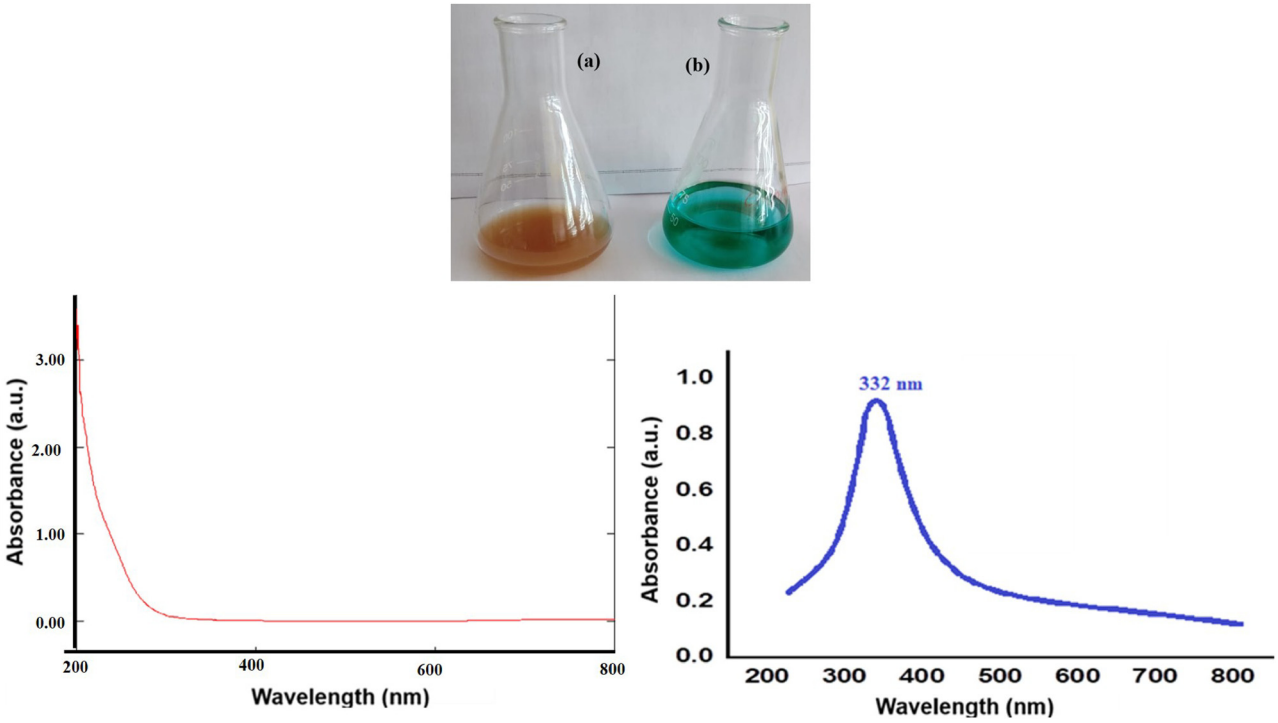

Figure 1: (a) Pumpkin seed extract showing a brownish color before reaction; (b) green coloration indicating the biosynthesis of Cu_4O_3 NPs after reaction with $CuSO_4$ solution. The UV–Vis spectrum (bottom left) of the plant extract shows no characteristic peak in the visible range, while the spectrum of the synthesized Cu_4O_3NPs (bottom right) displays a distinct absorption peak at 332 nm, confirming NP formation.

evaluate the influence of independent variables on the response. Analysis of variance (ANOVA) was performed with a 95% confidence level to determine the significance of the model and individual terms. The final regression equation, representing the relationship between variables and response, is presented in Section 3.

3 Results and discussion

3.1 UV–Vis spectroscopy

The color of the solution changed from brownish (Figure 1a) to green during the reaction, indicating the production of Cu_4O_3 NPs, allowing the bioreduction of $CuSO_4$ ions in the solution to be monitored. A 1 nm resolution UV–Vis spectroscopy at 200–800 nm further validated this transition. Analyzing the UV–Vis spectrum of the pumpkin seed extract reveals characteristic absorption peaks in the ultraviolet range, specifically between 220 and 380 nm. These absorptions are indicative of the presence of phenolic compounds and flavonoids, which are frequently found in plant extracts [77,78]. The UV–Vis spectra of Cu_4O_3NPs showed a distinctive surface plasmon resonance peak at 332 nm, which is indicative of the inherent band gap absorption of Cu_4O_3 brought on by electron transitions from the valence to the conduction band [79,80]. This absorption peak is significantly different from the typical absorption peaks of CuO (300–400 nm) and Cu_2O (250–350 nm). This peak is consistent with the reported interband transition of parahexachloride (Cu_4O_3, a mixed-valence Cu^+/Cu_2^+ oxide) [81]. The narrow peak width further confirms the formation of Cu_4O_3 NPs without CuO/Cu_2O impurities. This absorption peak is also notably distinct from those typically observed for CuO or metallic Cu, thereby supporting the identification of the product as Cu_4O_3. The sharp peaks also indicate that the particles are nanosized and have a narrow size distribution (Figure 1b). Notably, the UV–Vis spectra of both the freshly prepared and long-term stored Cu_4O_3 NPs were identical, further confirming that no significant changes occurred in their optical properties over time [32]. Briefly, based on the above discussion, the absorption peak in our work was observed at a longer wavelength of 332 nm. This red shift (shift to a longer wavelength) may be attributed to the formation of other metastable and stable copper oxide NPs with different electronic band structures.

3.2 FTIR spectroscopy analysis

FTIR spectra were recorded to identify the functional groups involved in the reduction and stabilization of Cu_4O_3 NPs synthesized using pumpkin seed extract (Figure 2a and b). The FTIR spectrum of pumpkin seed extract (Figure 2a) shows a broad band at 3363.49 cm^{-1}, corresponding to the O–H stretching vibration of hydroxyl groups, which are commonly found in alcohols and phenolic compounds. The peaks at 2923.15 and 2853.19 cm^{-1} are attributed to aliphatic C–H stretching vibrations, indicating the presence of $–CH_2$ and $–CH_3$ groups. The peak at 1668.96 cm^{-1} is attributed to the C═O stretching vibration (amide I), indicating the presence of amide compounds. The peaks at 1543.98 and 1461.84 cm^{-1} are associated with aromatic C═C stretching vibrations, while the peak at 1406.23 cm^{-1} is associated with O–H bending vibrations. The prominent band at 1156.40 cm^{-1} represents the C–O–C stretching vibrations within the polysaccharide. The peaks at 1078.09 and 1023.95 cm^{-1} are attributed to the C–O stretching vibrations of alcohols and ethers. The bands in the fingerprint region, such as those observed at 859.61 and

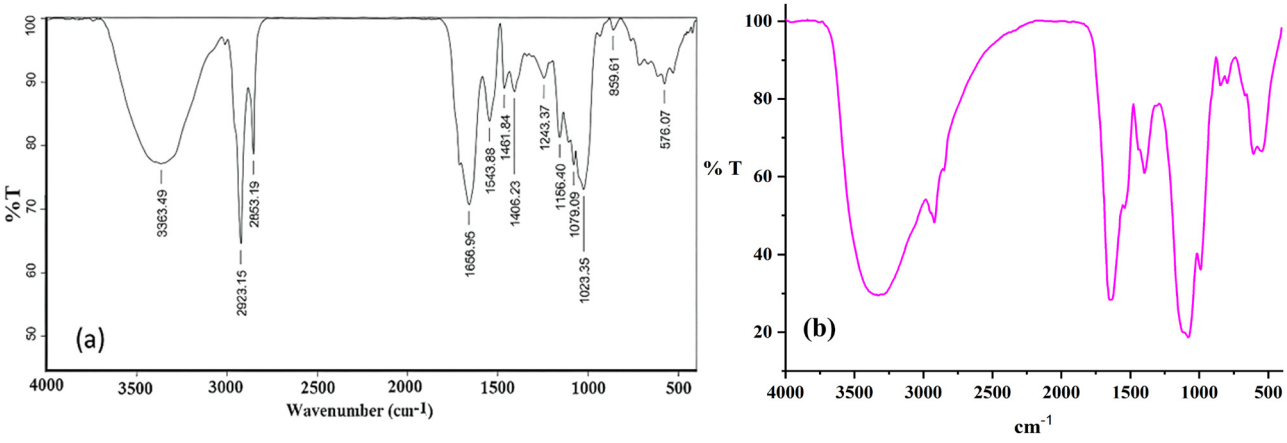

Figure 2: (a) FTIR spectrum of pumpkin seed extract, and (b) FTIR spectrum of Cu_4O_3NPs synthesized using pumpkin seed extract.

576.07 cm^{-1}, are typical features of out-of-plane bending modes and metal–oxygen bonds, respectively. In the FTIR spectrum of the synthesized Cu_4O_3 NPs (Figure 2b), similar functional groups were observed, but the peak positions were significantly shifted, indicating the interaction between the bioactive compounds in the extract and the NP surface. The O–H stretching vibration band appeared at 3328.58 cm^{-1}, and the aliphatic C–H stretching vibration bands were observed at 2959.02 and 2928.00 cm^{-1}, respectively. The C═O stretching vibration (amide I) shifted to 1648.40 cm^{-1}, while the aromatic C═C stretching vibration and O–H bending vibration bands were observed at 1547.83 and 1401.61 cm^{-1}, respectively. The peaks at 1082.30 and 1023.30 cm^{-1} confirmed the presence of C–O stretching vibrations associated with alcohols, ethers, esters, and carboxylic acids. Importantly, new peaks appeared in the lower wavenumber region at 553.92, 615.51, and 688.03 cm^{-1}, which correspond to Cu–O stretching vibrations, confirming the successful formation of Cu_4O_3 NPs [68]. The FTIR spectra of both the freshly prepared and long-term stored Cu_4O_3 NPs showed similar peak positions and intensities, indicating that no significant chemical changes occurred during storage. This suggests that the stability and surface composition of the NPs were maintained over time [32]. Together, these results suggest that the phytochemicals in the pumpkin seed extract not only play a key role in reducing copper ions but also act as stabilizers, forming a capping layer around the NPs. Additionally, by combining gas chromatography and mass spectrometry to confirm the presence of chemicals in the sample, eight compounds were found in the extract from pumpkin seeds [82], as detailed in Table 2. The NIST database was used for compound identification. These compounds include ethyl hexadecanoate, oleic acid, 9-octadecenoic acid, *cis*-octadecenoic acid, 9,12-octadecadienoic acid, 1-chloro-7-heptadecene, and 6,11-dimethyl-2,6,10-dodecatriene-1-ol.

3.3 Synthesis of copper oxide NPs using pumpkin seed extract: A mechanistic overview

The synthesis of copper oxide NPs (Cu_4O_3) using pumpkin seed extract involves a multifaceted process driven by the phytochemicals present in the extract, which function as both reducing and stabilizing agents. While the exact reaction mechanisms are complex and may involve multiple simultaneous pathways, a generalized framework of the likely chemical transformations can be proposed based on the existing literature and the bioactive compounds identified in pumpkin seed extract.

Table 2: Study on the active components of pumpkin seed extract

Compound	Molecular formula	Molecular formula	Figure
Octadecanoic acid or stearophanic acid	$C_{18}H_{36}O_2$	284	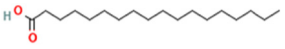
Oleic acid	$C_{18}H_{34}O_2$	282	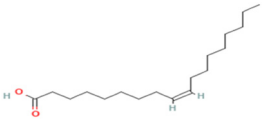
9-Octadecenoic acid	$C_{18}H_{34}O_2$	282	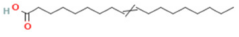
cis-Vaccenic acid	$C_{18}H_{34}O_2$	282	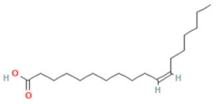
9,12-Octadecadeinoic acid	$C_{18}H_{32}O_2$	280	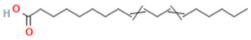
9,12-Octadecadeinoic acid	$C_{18}H_{32}O_2$	280	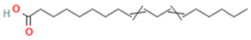
Oleic acid	$C_{18}H_{34}O_2$	282	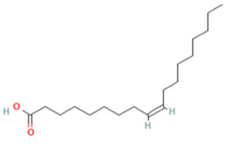
7-Heptadecene, 1-chloro	$C_{17}H_{33}Cl$	272	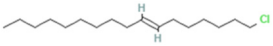
6,11-Dimethyl-2,6,10-dodecatrien-1-ol	$C_{14}H_{24}O$	208	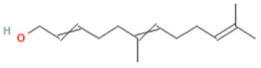
9,12-Octadecadeinoic acid	$C_{18}H_{32}O_2$	280	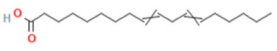

3.3.1 Reduction of copper ions (Cu^{2+} to Cu^0)

The process begins with the reduction of copper ions (typically derived from a precursor such as copper sulfate, $CuSO_4$) to metallic copper atoms (Cu^0). This transformation is facilitated by the reducing agents present in the pumpkin seed extract, which donate electrons to the Cu^{2+} ions. The general redox reaction can be represented as follows:

$$2Cu^{2+}\ (aq) + R\ (extract) \rightarrow 2Cu^{\circ}\ (s) + oxidized\ R\ (extract) + 2H^{+}\ (aq).$$

Here, R (extract) denotes the reducing components of the extract, which are oxidized during the reaction.

3.3.2 Nucleation and growth of copper NPs

Once reduced, the copper atoms undergo nucleation, forming small clusters that grow into NPs. This aggregation process can be expressed as

$$n Cu^{\circ}\ (s) \rightarrow (Cu)\ n\ (NP).$$

The size and morphology of the NPs are influenced by the kinetics of nucleation and growth, as well as the stabilizing effects of the organic molecules in the extract.

3.3.3 Oxidation to copper oxide (Cu_4O_3)

In the presence of dissolved oxygen, the metallic copper NPs are further oxidized to form copper oxide NPs, specifically Cu_4O_3. The oxidation reaction can be described as

$$4Cu^{\circ}\ (s) + 3/2O_2\ (g) \rightarrow Cu_4O_3(s).$$

This step highlights the role of oxygen in the final product formation.

The pumpkin seed extract plays a dual role in this synthesis process. Beyond its function as a reducing agent, it also acts as a stabilizing and capping agent. The organic molecules within the extract adsorb onto the surfaces of the growing NPs, preventing agglomeration and controlling their size and shape. Specific functional groups, such as hydroxyl (−OH), carboxyl (−COOH), and amino ($-NH_2$) groups, likely interact with the copper ions and NP surfaces through coordination bonds or electrostatic interactions. These interactions not only stabilize the NPs but also influence their physicochemical properties.

3.4 XRD pattern analysis

The XRD patterns of Cu_4O_3 NPs are shown in Figure 3a. The peak position is the same as that of standard Cu_4O_3, and the sharp peak creates a diffraction pattern that forms a crystal structure. The most intense diffraction peak at approximately $2\theta \approx 14°$ is indexed to the (112) plane ($d \approx 3.19$ Å), indicating it is the most preferentially oriented or most abundant plane in the sample. The additional peaks at 2θ values around 28°, 33°, 44°, and 56° are attributed to the (200) ($d \approx 2.75$ Å), (004) ($d \approx 2.34$ Å), (220) ($d \approx 2.01$ Å), and (224) ($d \approx 1.67$ Å) planes, respectively. These results are supportive of the standard JCPDS card no. 33-480 and the literature [68], confirming the presence of tetragonal copper oxide paramelaconite. Thus, the well-known

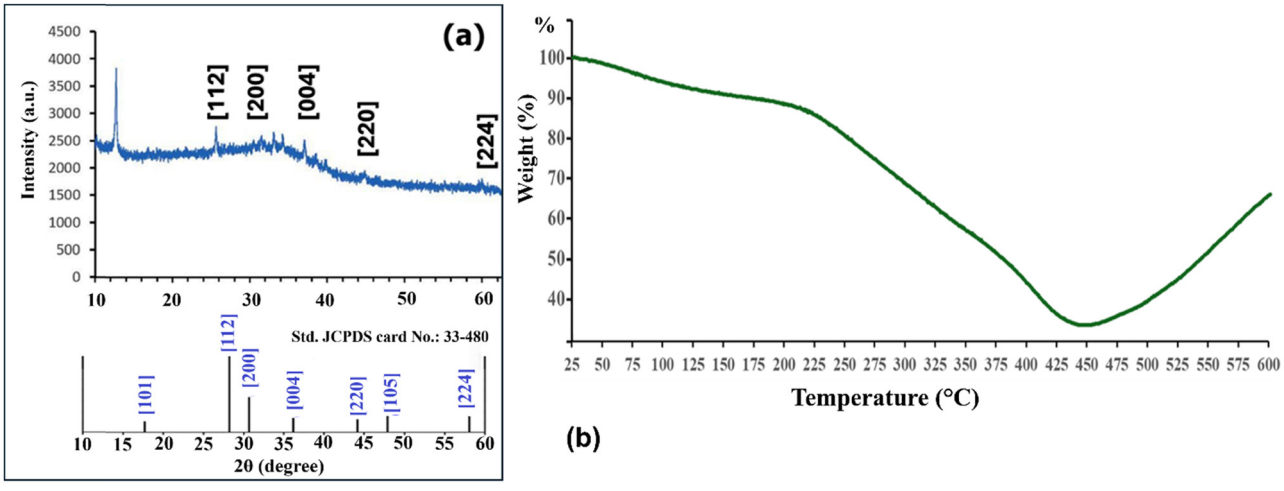

Figure 3: (a) XRD pattern of Cu_4O_3 NPs, matching with JCPDS card no. 33-0480, confirming the crystalline nature of the Cu_4O_3 phase. (b) TGA plot of weight loss *versus* temperature.

Debye–Scherrer equation ($D = K\lambda/\beta\cos\theta$) was used to determine the average crystalline size of the Cu_4O_3NPs. In the above equation, D is the particle size (nm), λ is the wavelength of the X-ray source, K is a constant (0.94), β is the peak half-width (rad), and 2θ is the Bragg angle. The high-intensity peak for the analysis indicated a crystalline size of 16 nm in the peak plane of the XRD pattern.

To evaluate the purity of the synthesized Cu_4O_3 NPs, XRD data, EDX, alongside TGA were analyzed. The XRD results confirmed the formation of pure Cu_4O_3 with no detectable impurities, as evidenced by the absence of prominent additional peaks corresponding to other phases or contaminants. However, it is important to note that while the inorganic phase (Cu_4O_3) is highly pure, the NPs may still contain residual organic material from the pumpkin seed extract, which serves as a stabilizing agent. This organic material is not detrimental to the crystallinity of the NPs but contributes to their colloidal stability and prevents agglomeration.

3.5 TGA

TGA provided further insights into the purity of the synthesized Cu_4O_3 NPs. The TGA curve revealed distinct stages of weight loss, which can be attributed to the removal of volatile components and organic residues. In the initial stage (30–150°C), a weight loss of 9.7% was observed, primarily due to the evaporation of water and low-molecular-weight organic compounds. The second stage (150–220°C) showed an additional weight loss of 12.7%, corresponding to the decomposition of more complex organic molecules from the pumpkin seed extract. These two stages collectively indicate that approximately 22.4% of the total weight corresponds to organic material and moisture, leaving behind the inorganic Cu_4O_3 phase. Beyond 220°C, the gradual weight loss up to 450°C (total decrease of 80.17%) is attributed to the continued breakdown of residual organics and the phase transition of Cu_4O_3. Finally, in the temperature range of 450–600°C, an increase in weight of 65% was observed, likely due to oxidation processes leading to the formation of higher copper oxides. These results confirm that the NPs retain some organic content for stabilization, while the residual inorganic phase is predominantly Cu_4O_3, as supported by the XRD data. Thus, the TGA provides quantitative evidence of the high purity of the Cu_4O_3 phase, with controlled retention of organic material to ensure NP stability.

3.6 FESEM analysis

Scanning electron microscopy (SEM) was used to study the surface morphology of the synthesized Cu_4O_3 NPs at different magnifications. At lower magnification, SEM images show a uniform distribution of particles. However, the resolution is not enough to distinguish the boundaries of individual grains. The surface morphology of NPs, including the presence of monodisperse particle clusters and formed aggregates, can be observed using high-magnification imaging. These data imply that gravity causes uniformly distributed particles to initially coalesce into clusters. Based on SEM analysis, the average particle size was found to be about 1 µm (Figure 4a). The elemental composition of the synthesized NPs was analyzed using EDX spectroscopy (Figure 4b). The EDX spectrum confirmed the presence of copper (Cu) and oxygen (O) as the primary elements, with significant signals corresponding to 47.1 at% Cu and 40.6 at% O. The detection of only Cu and O in significant quantities suggests a relatively high purity of the

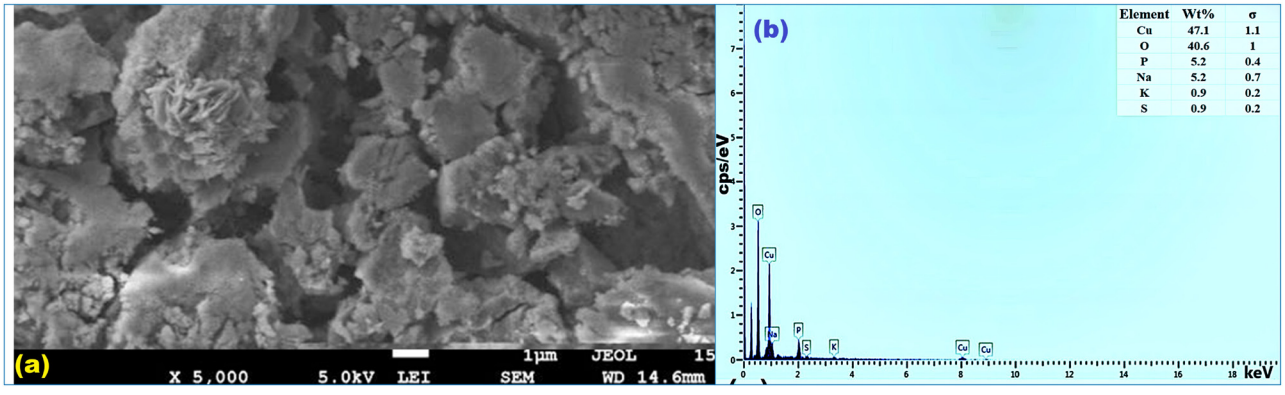

Figure 4: (a) SEM micrograph and (b) EDX spectrum of Cu_4O_3 NPs.

synthesized Cu_4O_3 NPs. The atomic ratio of Cu to O is approximately 1.16:1, which is close to the theoretical ratio of 4:3 (1.33:1) for Cu_4O_3, considering potential surface oxidation or minor variations. The presence of minor peaks corresponding to other elements such as Na (1.0%), P (5.2%), S (0.7%), Cl (0.8%), and K (0.7%) indicates the presence of trace amounts of residues likely originating from the pumpkin seed extract used in the synthesis process. While these impurities are present in small quantities, the dominant signals of Cu and O confirm that the synthesized product is predominantly copper oxide.

3.7 HRTEM of Cu_4O_3 NPs

The fabricated Cu_4O_3 NPs were characterized using transmission electron microscopy (TEM). The scale bar in the TEM image corresponds to a field-of-view width of 100 nm. The NPs exhibited a range of morphologies, including spherical, oval, and irregular shapes. Additionally, blocky or rounded morphologies with protrusions were observed. The NPs' diameter ranged from 20 to 100 nm, with some evidence of aggregation, as shown in Figure 5a. The TEM analysis determined the size, which roughly agreed with the Scherrer equation's estimate. This observation supports the successful formation of Cu_4O_3 NPs using aqueous pumpkin seed extracts in the present study. High-resolution TEM analysis revealed a thin, amorphous layer surrounding the Cu_4O_3 NPs. This layer is made up of organic material from aqueous extracts, which may serve as a capping agent for the NPs. The selected area electron diffraction (SAED) pattern in Figure 5b indicates that the biofabricated Cu_4O_3 NPs have a partially crystalline structure. The SAED pattern's diffraction rings match that of the tetragonal copper oxide paramelaconite, which is in line with the XRD results and adds to the reliability of the characterization. The particle size distribution of Cu_4O_3 NPs synthesized using pumpkin seed extract was analyzed, and the histogram (Figure 5c) reveals a mean particle size of 26.463 nm. The size range was found to be between approximately 8.92 and 55.84 nm, indicating a relatively uniform distribution with most particles concentrated between 20 and 35 nm. These data, consistent with TEM analysis, confirm the nanoscale nature of the synthesized particles and suggest effective capping and stabilization by the phytochemicals present in the extract.

3.8 Optimization of Cu_3O_4 NP synthesis from pumpkin seed extract using BBD

The optimization of Cu_4O_3 NP synthesis using pumpkin seed extract was carried out using the BBD. This approach allowed for a systematic evaluation of the impact of key process variables on the synthesis. The independent factors studied were precursor concentration (A), reaction temperature (B), and reaction time (C). By varying these factors, their influence on both the yield and properties of the NPs was thoroughly analyzed (Table 3). The experimental design matrix and the resulting response values were assessed using ANOVA to determine the statistical significance of the factors and to evaluate the adequacy of the model.

The optimization of Cu_4O_3 NP synthesis using pumpkin seed extract was systematically investigated using the BBD. The effects of three independent variables (Tables 1 and 3) were evaluated to understand their influence on the yield and properties of the NPs. The experimental data were

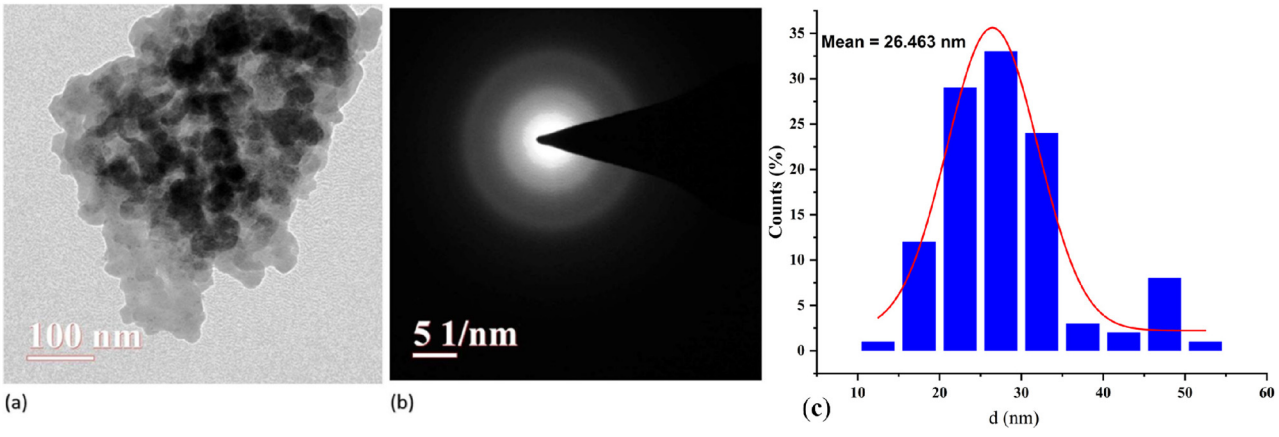

Figure 5: (a) TEM image of Cu_4O_3 NPs at a field of view width of 100 nm, (b) corresponding SAED pattern, and (c) particle size distribution of Cu_4O_3 NPs with a mean size of 26.463 nm, indicating a relatively narrow range, with most particles falling between 20 and 35 nm.

Table 3: Optimization of Cu_4O_3 NP biosynthesis using BBD

Run	$CuSO_4$ concentration (mM)	Extract volume (mL)	Reaction temperature (°C)	Yield (%)
1	3.0	10.0	85	60
2	7.0	10.0	85	72
3	3.0	30.0	85	68
4	7.0	30.0	85	80
5	5.0	20.0	85	66
6	5.0	20.0	110	78
7	5.0	10.0	97	65
8	5.0	30.0	97	84
9	3.0	20.0	97	62
10	7.0	20.0	97	88
11	5.0	10.0	110	70
12	5.0	30.0	110	86
13	3.0	20.0	110	64
14	7.0	20.0	110	90
15	5.0	20.0	97	75

analyzed using ANOVA to assess the statistical significance of the factors and the adequacy of the model. Figure 6(a) presents the Pareto chart of standardized effects for yield (%), with a significance level of $\alpha = 0.05$. The graph illustrates the relative importance of each term in the model, including the main factors (A, B, C), their quadratic terms (AA, BB, CC), and interaction terms (AB, AC, BC). The length of each bar corresponds to the size of the standardized effect, with a reference line indicating the threshold for statistical significance. This analysis helps identify the most influential factors and interactions that affect the yield of NPs. The normal probability plot of the residuals is shown in Figure 6b, evaluating the model's normality assumption. Based on the plot, it appears that the residuals are roughly straight lines, indicating that the errors are normally distributed and that the assumptions of the model are valid. Figure 6c shows the histogram of residuals to illustrate their distribution visually. Using the histogram, we can see that the residuals are centered around zero with no skewness or outliers, thus confirming the validity of the model. As shown in Figure 6d, the residuals *versus* fitted values plot checks for homoscedasticity (constant residual variance). Across the range of fitted values, the residuals around the zero line are distributed randomly, confirming the model's reliability. Figure 6e shows the independence of residuals over time by plotting residuals *versus* the order of observations. As the pattern of residuals shows no systematic trend or autocorrelation, the experimental runs were conducted under steady-state conditions. The RSM analysis revealed the individual and interactive effects of the selected parameters on performance. The contour plots (Figure 6f and g) demonstrated that elevating the concentration of $CuSO_4$ and the volume of pumpkin seed extract led to enhanced production, with optimal yield observed at intermediate levels of both parameters. The impact of reaction temperature was evident, exhibiting an increase in the yield until an optimal threshold was attained, after which a decline occurred, indicating possible heat degradation of bioactive compounds that stabilize the NPs. The 3D response surface plot (Figure 6h) corroborated the curvature in the response, signifying a strong interaction between the components. The quadratic model indicated that both linear and quadratic effects significantly influenced NP performance. Figure 6i shows that a maximum yield of 89.87% was obtained at 105.71°C using 16.26 mL of pumpkin seed extract and 7.0 mM $CuSO_4$. The optimum was determined by a BBD. The model had a desirability score of 0.9956, indicating its accuracy in predicting the optimal response. The maximum yield was achieved within the specified limits, confirming the efficacy of the biogenic synthesis under regulated conditions.

Table 4 provides a more comprehensive description. The elevated *R*-squared number suggests that the model is significant overall, although this is not definitively proven. The individual linear effects of $CuSO_4$ concentration, extract volume, and temperature were not statistically significant. Changing any one factor alone, while holding the others constant, did not have a statistically significant effect on the yield within the range examined.

Table 4 highlights the significant influence of the interaction between $CuSO_4$ concentration and extract volume ($p = 0.035$). This indicates that the impact of $CuSO_4$ concentration on yield is significantly influenced by the volume of extract employed and *vice versa*. Enhancing one aspect without accounting for the other would be inadequate. This interaction facilitates the high projected yield depicted in Figure 6i at the precise combination of 7.0 mM $CuSO_4$ and 16.26 mL extract, despite the distinct linear effects being insignificant independently. The marginal *p*-value for the quadratic term of the extract volume ($p = 0.051$) further substantiates the intricate link between the extract volume and yield, indicating a non-linear influence. The lack-of-fit *p*-value of 0.099 in Table 4 indicates that the model, while beneficial, may not entirely represent all the intricacies of the system. This may result from a minor factor excluded from the model or slight departures from the presumed quadratic relationship. Notwithstanding this, the model effectively discerned a practically advantageous optimum, as demonstrated by the elevated desire and the recorded maximum yield. Using pumpkin seed extract, the BBD approach significantly improves the NP synthesis conditions. Collectively, these evaluation plots confirm the robustness of the BBD and the suitability of the

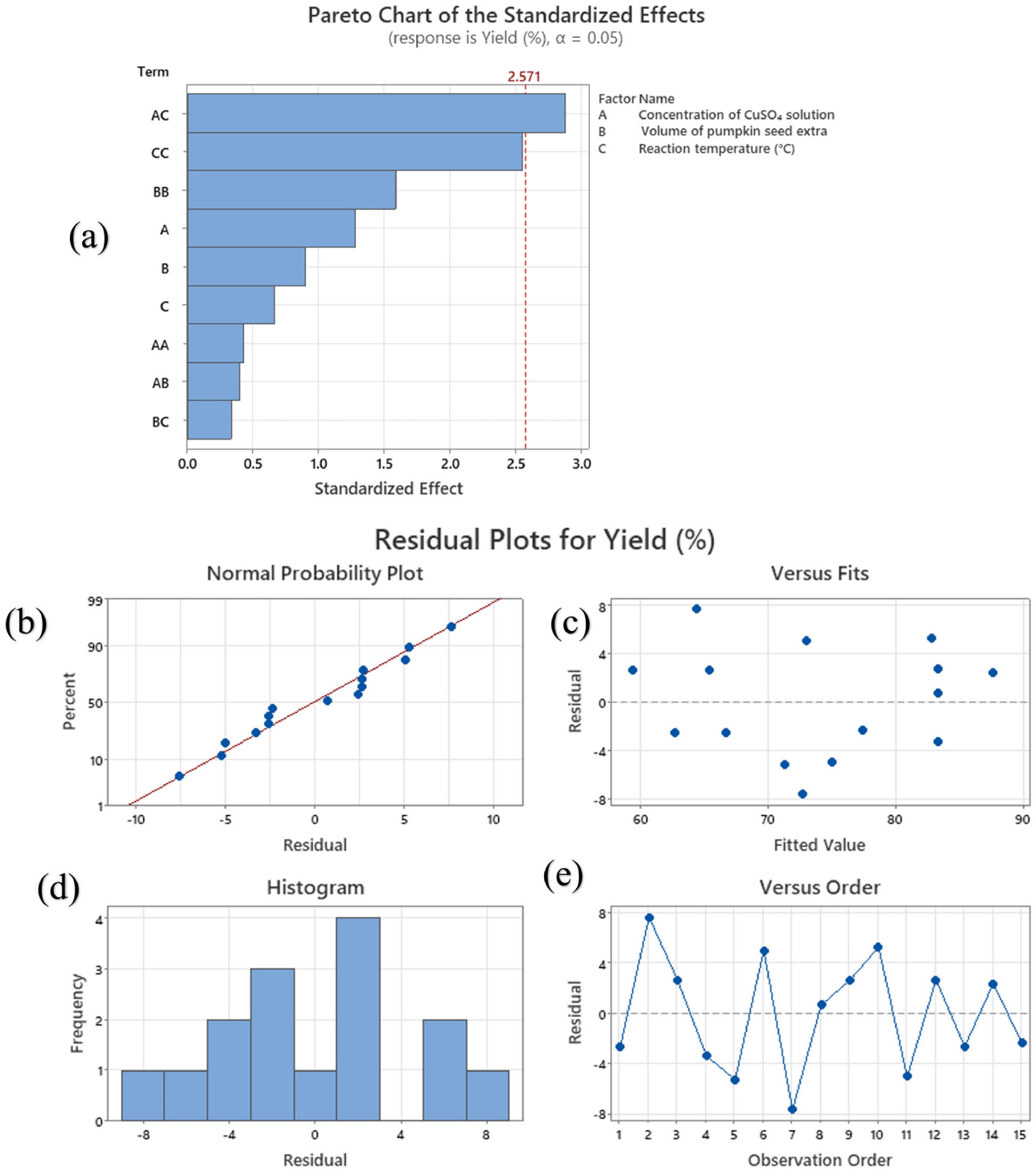

Figure 6: Statistical analysis of Cu_3O_4 NP synthesis optimization using a BBD. (a) The Pareto chart identifies significant effects, with bars exceeding the red line (α = 0.05), indicating statistical significance. (b) The normal probability plot assesses residual normality, with points expected along the diagonal line. (c) The residuals *vs* fitted values plot checks for constant variance. (d) The histogram further evaluates residual normality. (e) The residuals *vs* observation order plot examines potential time-related trends. Response surface plots showing the influence of $CuSO_4$ concentration, extract volume, and reaction temperature on the Cu_3O_4 NP yield. (f) $CuSO_4$ concentration *vs* extract volume. (g) $CuSO_4$ concentration *vs* reaction temperature. (h) 3D plot of $CuSO_4$ concentration *vs* extract volume. (i) Individual factor effects on Cu_3O_4 NP yield at the optimal setting.

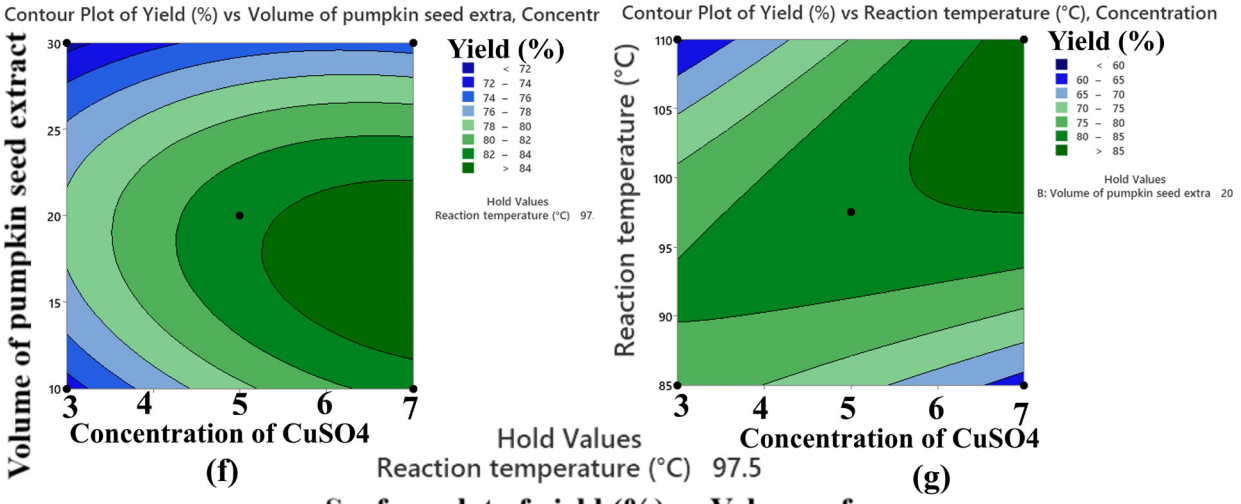

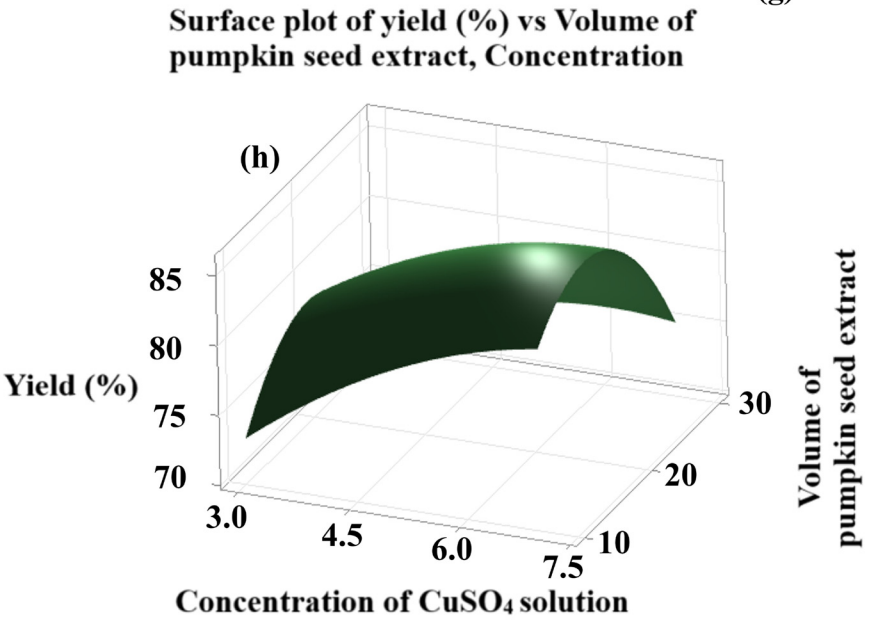

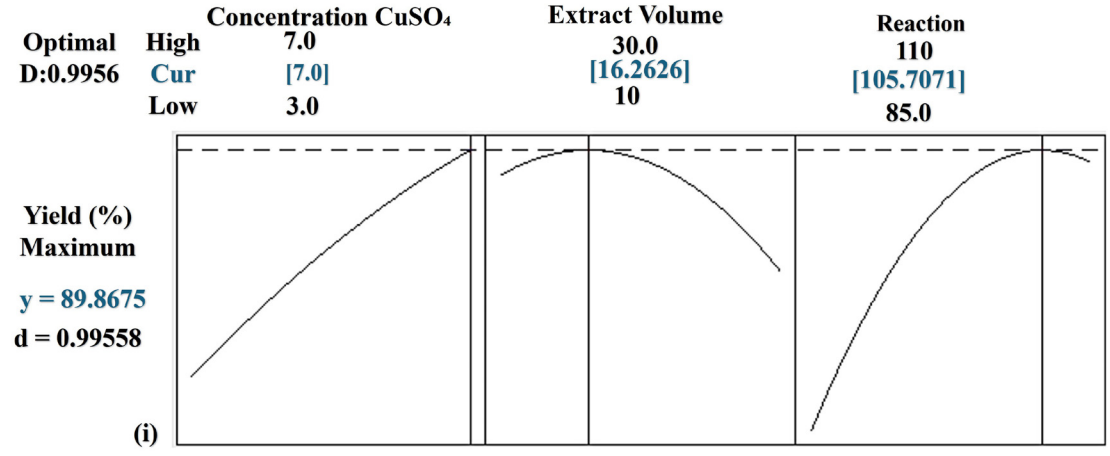

Figure 6: (*Continued*)

Table 4: ANOVA for optimizing Cu_3O_4 NP synthesis with BBD

Source	DF	Adj SS	Adj MS	*F*-value	*P*-value
Model	9	1110.82	123.424	2.21	0.198
Linear	3	160.75	53.583	0.96	0.479
Concentration of $CuSO_4$ solution	1	91.12	91.125	1.63	0.257
Volume of pumpkin seed extra	1	45.12	45.125	0.81	0.410
Reaction temperature (°C)	1	24.50	24.500	0.44	0.537
Square	3	472.57	157.522	2.82	0.146
Concentration of $CuSO_4$ solution*concentration of $CuSO_4$ solution	1	10.26	10.256	0.18	0.686
	1	140.41	140.410	2.52	0.173
Volume of pumpkin seed extra*volume of pumpkin seed extract	1	363.10	363.103	6.51	0.051
Reaction temperature (°C)*reaction temperature (°C)	3	477.50	159.167	2.85	0.144
2-way interaction	1	9.00	9.000	0.16	0.705
Concentration of $CuSO_4$ solution*volume of pumpkin seed extract	1	462.25	462.250	8.29	0.035
Concentration of $CuSO_4$ solution*reaction temperature (°C)	1	6.25	6.250	0.11	0.751
Volume of pumpkin seed extract*reaction temperature (°C)	5	278.92	55.783		
Error	3	260.25	86.750	9.29	0.099
Lack-of-fit	2	18.67	9.333		
Pure error	14				
Total					

quadratic model to optimize the synthesis of Cu_4O_3 NPs. The insights gained from this analysis provide a solid foundation for further optimization and scaling.

3.9 Statistical analysis

The experiments were designed and analyzed using MiniTab Statistical Software (Minitab LLC, Pennsylvania, USA). A full quadratic model was employed for data analysis, and ANOVA was performed with a 95% confidence level. The quadratic regression model is shown as follows: Regression Equation in Uncoded Units Yield (%) = −390 − 34.6 concentration of $CuSO_4$ solution + 3.58 volume of pumpkin seed extract + 10.57 reaction temperature (°C) − 0.417 concentration of $CuSO_4$ solution × concentration of $CuSO_4$ solution − 0.0617 volume of pumpkin seed extract × volume of pumpkin seed extract − 0.0635 reaction temperature (°C) × reaction temperature (°C) − 0.075 concentration of $CuSO_4$ solution × volume of pumpkin seed extract + 0.430 concentration of $CuSO_4$ solution × reaction temperature (°C) − 0.0100 volume of pumpkin seed extract × reaction temperature (°C).

3.10 MTT assay

The cytotoxicity of biogenic Cu_4O_3 NPs against human lung adenocarcinoma (A549) and colon cancer (HCT-116) cell lines was evaluated using the MTT assay (Figure 7). The assay measures the activity of mitochondrial succinate dehydrogenase, an enzyme that is an indicator of cell viability. The results showed that the cell viability of both cell lines decreased in a dose-dependent manner with increasing concentrations of Cu_4O_3 NPs (ranging from 0 to 1,280 µg/mL). The calculated IC_{50} values, which represent the concentration required to inhibit 50% cell viability, were 402.37 µg/mL for A549 cells and 449.32 µg/mL for HCT-116 cells. The biogenic Cu_4O_3 NPs exhibited an IC_{50} of 11 µg/mL against HCT-116 cells when freshly prepared [32]. Statistical analysis of the differences in cell viability between the two cell lines at each concentration is provided in Figure 7. However, after long-term storage, the IC_{50} increased substantially to 449.32 µg/mL when the sample was retested, indicating a reduction in cytotoxic efficacy. These values indicate that the synthesized Cu_4O_3 NPs exhibited a higher cytotoxic effect against A549 lung cancer cells than against HCT-116 colon cancer cells. These results are consistent with other studies investigating the cytotoxic potential of Cu_4O_3 NPs, although specific IC_{50} values may vary depending on the synthesis method, NP characteristics (size, morphology, and surface properties), and the cell line tested. For instance, Jabir *et al.* [83] reported a significantly lower IC_{50} value of 9.5 µg/mL for Cu_4O_3 NPs against the PA-1 human ovarian cancer cell line. This higher efficacy in PA-1 cells could be attributed to differences in cellular uptake mechanisms or specific interactions between the NPs and the PA-1 cell line. This higher efficacy in PA-1 cells may be attributed to differences in the

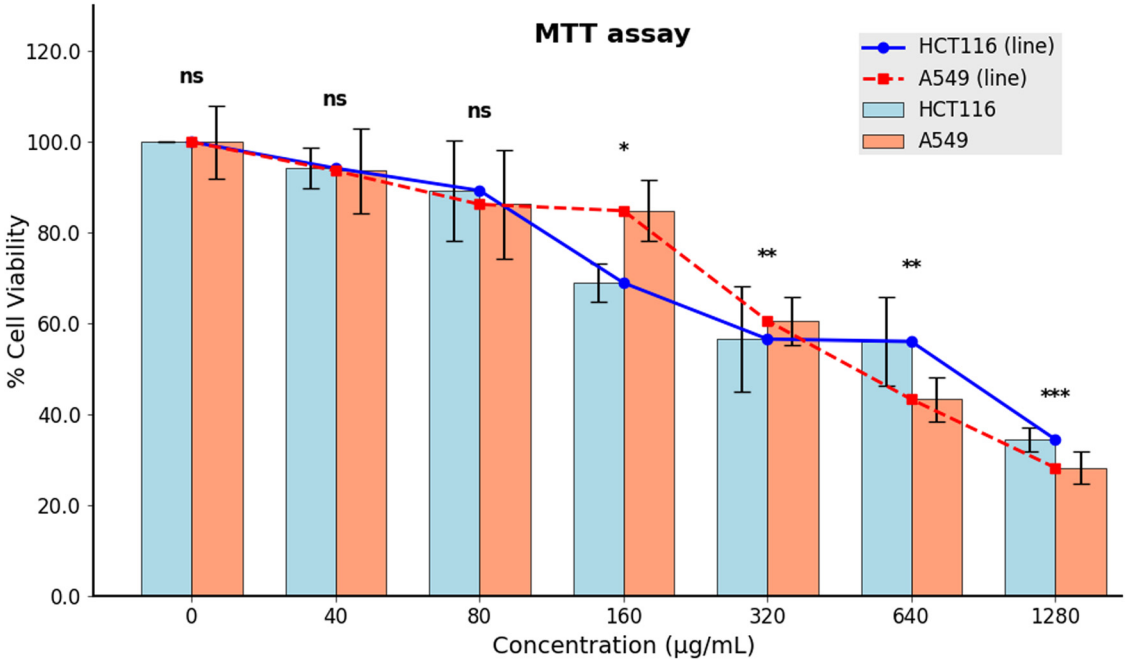

Figure 7: Dose-dependent cytotoxic effect of biofabricated Cu_4O_3 NPs on HCT-116 and A549 cancer cell lines assessed by MTT assay. Cells were treated with increasing concentrations (0–1,280 µg/mL) of Cu_4O_3 NPs for 24 h. Data represent mean ± SD of triplicate measurements. Statistical significance between HCT-116 and A549 at each concentration was evaluated (*$p < 0.05$, **$p < 0.01$, ***$p < 0.001$; ns = not significant).

cellular uptake mechanism or specific interactions between the NPs and the PA-1 cell line. Similarly, another study [68] examined the effects of Cu_4O_3 NPs on PC-3 human prostate cancer cell lines and normal NIH/3T3 cell lines. While the study reported dose-dependent cell growth arrest in PC-3 cells, cytotoxicity data in normal cells were also provided, which is critical for evaluating the potential therapeutic window of these NPs. The moderate cytotoxic effect observed in our study, with IC_{50} values in the range of hundreds of µg/mL, suggests that while the biogenic Cu_4O_3 NPs are active against these cancer cell lines, higher concentrations may be required for significant inhibition compared to other reports. The differences in IC_{50} values between studies highlight the importance of considering the specific characteristics of the NPs and cell lines used in the evaluation. Our study focused on two cancer cell lines, and future work could explore the selectivity of our bioderived Cu_4O_3 NPs by performing analyses in normal cell lines to evaluate their potential in cancer-targeted therapy. Although the IR spectra, EDX profiles, and

Table 5: Antibacterial activity of biogenic Cu_4O_3NPs, demonstrating the zone of inhibition on discs

Concentration of Cu_4O_3 NPs (ppm)	*B. subtilis*; inhibition zone diameter			
	Cu_4O_3 NPs NZI (cm)	Standard (30 mcg)	NC NZI (cm)	
1	1.7 ± 0.1	3.0 ± 0.1	0 ± 0	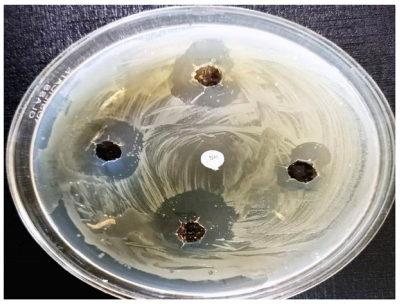
2	1.9 ± 0.1			
3	2.4 ± 0.05			
4	2.8 ± 0.06			

NZI: no zone of inhibition; NC: negative control. The results are reported as mean ± SD ($n = 3$).

Table 6: Comparative overview of Cu_4O_3 NP studies

NPs	Extract	Characterization	Size/morphology	Assay	Refs.
Cu_4O_3	Razma seed	XRD, FTIR, UV–Vis (270 and 372 nm), SEM and TEM	27 nm, sponge	Antibacterial, cytotoxic, antioxidant	[68]
	Pumpkin seeds	UV–Vis (332 nm), FTIR, EDX, HR-TEM, TGA	>100 nm, spherical, large, irregular, and agglomerated forms	Cytotoxicity	[32]
	Pumpkin seeds	SEM, TEM	<100 nm, spherical shape	Cytotoxicity assay, morphological alteration, induction of apoptosis	[83]
	Aloe barbadensis	UV (200–300 nm), FTIR, XRD, SEM	≈200 nm, tetragonal	Antibacterial, fungal	[86]
	Aegle marmelos leaf	UV–Vis, SEM, DLS, XRD, FTIR	~200 nm	Antibacterial	[87]
CuO	*Spinacia oleracea* leaf	UV–Vis (270 nm), XRD, EDX, and SEM	Avg. PS: 134.8 nm, Ovals, spheres, hexagons, cubes	Antioxidant, antibacterial, larvicidal and biosafety assay	[88]

TGA thermograms of the stored NPs were superimposable with those of the fresh samples [32], indicating no major chemical, elemental, or thermal changes, characterization revealed significant aggregation. This aggregation likely reduced dispersion and surface area, impairing cellular uptake and leading to diminished biological activity [84]. These findings highlight the critical role of NP stability and storage conditions in preserving cytotoxic efficacy. Aggregation of NPs can decrease surface reactivity and hinder cellular internalization, which are crucial factors affecting their therapeutic potential. Therefore, strategies to prevent aggregation or improve redispersion after storage should be considered to maintain biological activity.

3.11 Antibacterial activity analysis of NPs

This study examined the antibacterial effectiveness of Cu_4O_3 NPs against the Gram-positive bacterium *Bacillus subtilis*. Table 5 demonstrates the formation of distinct regions devoid of development around wells containing Cu_4O_3 NPs, suggesting their inhibitory effect on *B. subtilis*. As the concentration of NPs increased from 1 to 4 ppm, the effectiveness of NPs increased (Table 5). The absence of bacterial growth in these clear zones indicates the antibacterial impact of the NPs. The findings additionally indicate that the NPs engage with and exert a potent impact on *B. subtilis* cells. The Cu_4O_3 NPs exhibit a larger diameter of the zone of inhibition, which is a quantitative indicator of antibacterial activity, in comparison to tetracycline (30 mcg, standard) [85]. These findings indicate that Cu_4O_3 NPs have a more potent antibacterial effect against *B. subtilis* compared to the reference material. The minimum inhibitory concentration (MIC) of biosynthesized Cu_4O_3 NPs was found to be 3 ppm against *B. subtilis*, as this was the lowest concentration that completely inhibited visible bacterial growth in the broth dilution assay.

3.12 Relating to existing work

The synthesis and characterization of Cu_4O_3 NPs were reported in previous studies, as summarized in Table 6.

Our green synthesis approach utilizing pumpkin seed extract offers a potentially more sustainable and cost-effective alternative to some conventional methods. The characteristic UV–Vis absorption peak observed at 332 nm in our study aligns with the reported interband transition for Cu_4O_3, although the specific wavelength can vary

slightly depending on factors such as particle size and synthesis conditions. The morphology and size of the synthesized Cu_4O_3 NPs in our work were predominantly spherical with sizes ranging from 8.92 to 55.84 nm, showing a different size profile compared to other reports. For instance, Table 6 reports a larger size of Cu_4O_3 NPs with sizes ranging from 27 nm (sponge-like morphology) to >100 nm (spherical, large, irregular, and agglomerated forms), <100 nm (spherical shape), ≈200 nm (tetragonal), and ~200 nm (hexapod morphology). These differences in size and morphology could influence the surface area and, consequently, the observed properties. Our investigation into the cytotoxicity of the pumpkin seed extract-mediated NPs on HCT-116 and A549 cell lines provides insights into their potential biomedical applications. While some previous studies on Cu_4O_3 NPs have explored properties like antibacterial and anticancer activities, our findings specifically contribute to the understanding of their cytotoxic effects on these cancer cell lines. Further research directly comparing the antibacterial and cytotoxic activities of Cu_4O_3 NPs synthesized through different routes and exhibiting varying sizes would be beneficial. The present study contributes to the growing body of literature on copper oxide NPs by offering a green synthesis route using a plant extract and providing valuable data on their size distribution and cytotoxic potential against specific cancer cell lines. The comparative analysis with existing reports highlights both the consistency of our UV–Vis identification of the copper oxide and the unique size characteristics of the NPs produced through our method and their investigated bioactivity.

3.13 Molecular index analysis

The calculated HOMO–LUMO energy gap (ΔE = 1.23 eV) suggests a moderate chemical reactivity. While a smaller gap typically indicates higher reactivity, this value still implies a potential for interaction with biological systems through electron transfer processes. The electronegativity (χ = 4.218 eV) indicates the tendency of the Cu_4O_3 cluster to attract electrons, which could be relevant in interactions with bacterial cell walls or cancer cell membranes. The chemical hardness (η = 0.613 eV) and softness (S = 0.816 eV^{-1}) provide further insights into the cluster's stability and polarizability. A higher hardness implies greater resistance to deformation of the electron cloud, while a higher softness indicates greater polarizability and, thus, potentially stronger interactions with biological molecules (Table 7 and Figure 8).

Considering the observed antimicrobial activity against *B. subtilis* and cytotoxicity against A549 and HCT-116 cell lines, the moderate reactivity indicated by our DFT calculations suggests that the Cu_4O_3 NPs can interact with biological targets. The specific mechanisms likely involve a combination of factors, including the release of copper ions, the generation of reactive oxygen species, and direct interactions of the NP surface with biomolecules. The electronic properties, particularly the electronegativity and softness, could influence the NP's affinity for and interaction with cellular components. Further experimental studies are needed to fully elucidate these mechanisms, but these computational insights provide a valuable foundation for understanding the inherent reactivity of the Cu_4O_3 NPs and their potential for biological activity.

Table 7: Molecular indices: calculated global reactivity descriptors for Cu_4O_3

Property	Value (eV)	Formula
HOMO energy (E_{HOMO})	−4.830	Direct from orbital energies
HOMO energy (E_{LUMO})	−3.605	Direct from orbital energies
Energy gap (ΔE)	1.23	$E_{LUMO} - E_{HOMOE}$
Ionization potential (IP)	4.830	$-E_{HOMOE}$
Electron affinity (EA)	3.605	$-E_{LUMO}$
Electronegativity (χ)	4.218	(IP + EA)/2
Chemical hardness (η)	0.613	(IP − EA)/2
Chemical softness (S)	0.816	$1/(2\eta)$

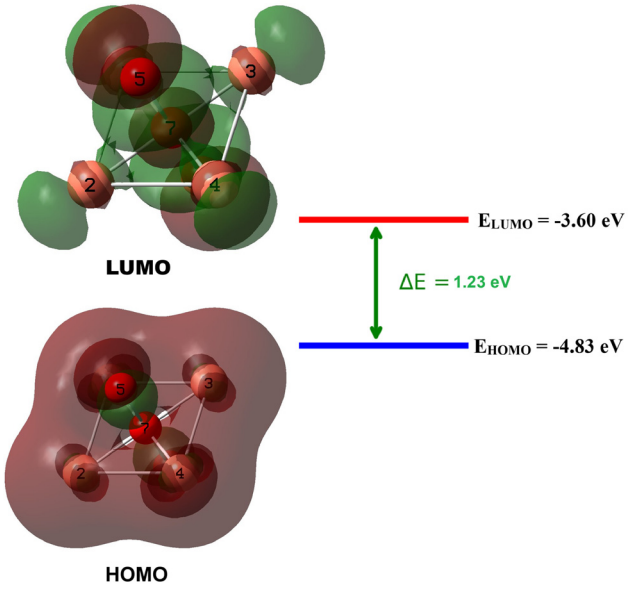

Figure 8: HOMO and LUMO orbitals of the optimized Cu_4O_3 cluster, showing their respective energies.

4 Conclusion

In this study, we successfully demonstrated a green, sustainable approach for synthesizing Cu_4O_3 NPs using pumpkin seed extract as a biogenic reducing, stabilizing, and capping agent. Physicochemical characterization confirmed the formation of crystalline Cu_4O_3 NPs with sizes ranging from 8.92 to 55.84 nm. Optimization using the BBD highlighted the significant influence of the reaction temperature and extract volume on the NP yield, achieving a maximum predicted yield of 89.87%. This biosynthesis route presents an innovative and eco-friendly alternative to conventional chemical methods, leveraging the rich bioactive profile of pumpkin seeds. Computational studies employing DFT elucidated the electronic structure of the Cu_4O_3 cluster, revealing a moderate HOMO–LUMO energy gap indicative of potential interactions with biological systems. Compared with previous studies that used different plant extracts, our approach not only produced NPs with favorable morphology and crystallinity but also demonstrated notable biological activities. The synthesized Cu_4O_3 NPs exhibited moderate cytotoxicity against A549 and HCT-116 cancer cell lines and antibacterial efficacy against *B. subtilis*, suggesting potential applications in biomedicine. The findings validate our initial hypothesis that pumpkin seed extract could facilitate efficient NP synthesis with promising biological functionality. Future studies should explore the cytocompatibility of these NPs with normal cells, detailed mechanistic studies of cytotoxicity, and the expansion of this green synthesis strategy to other medically relevant metal oxide NPs.

Acknowledgments: This study was supported by the National Disaster Management Research Institute under the project “Disaster Forecasting and Warning System Integration Standards and Technology Development” (NDMI-2025-03-04). We express our gratitude for their support.

Funding information: The National Disaster Management Research Institute under the project “Disaster Forecasting and Warning System Integration Standards and Technology Development” (NDMI-2025-03-04).

Author contributions: All authors have accepted responsibility for the entire content of this manuscript and approved its submission.

Conflict of interest: The authors state no conflict of interest.

Data availability statement: All data generated or analyzed during this study are included in this published article.

References

[1] Ma X, Tian Y, Yang R, Wang H, Allahou LW, Chang J, et al. Nanotechnology in healthcare, and its safety and environmental risks. J Nanobiotechnol. 2024;22(1):715.
[2] Luther DC, Huang R, Jeon T, Zhang X, Lee YW, Nagaraj H, et al. Delivery of drugs, proteins, and nucleic acids using inorganic nanoparticles. Adv Drug Deliv Rev. 2020;156:188–213.
[3] Deka K, Nongbet RD, Das K, Saikia P, Kaur S, Talukder A, et al. Understanding the mechanism underlying the green synthesis of Metallic nanoparticles using plant extract (s) with special reference to Silver, Gold, Copper and Zinc oxide nanoparticles. Hybrid Adv. 2025;9:100399.
[4] kazemi S, Hosseingholian A, Gohari SD, Feirahi F, Moammeri F, Mesbahian G, et al. Recent advances in green synthesized nanoparticles: From production to application. Mater Today Sustain. 2023;24:100500.
[5] Sati A, Ranade TN, Mali SN, Ahmad Yasin HK, Pratap A. Silver nanoparticles (AgNPs): comprehensive insights into bio/synthesis, key influencing factors, multifaceted applications, and toxicity – A 2024 update. ACS Omega. 2025;10(8):7549–82.
[6] Malaikolundhan H, Mookkan G, Krishnamoorthi G, Matheswaran N, Alsawalha M, Veeraraghavan VP, et al. Anticarcinogenic effect of gold nanoparticles synthesized from Albizia lebbeck on HCT-116 colon cancer cell lines. Artif Cells Nanomed, Biotechnol. 2020;48(1):1206–13.
[7] Baral J, Pokharel N, Dhungana S, Tiwari L, Khadka D, Pokhrel MR, et al. Green synthesis of copper oxide nanoparticles using Mentha (Mint) leaves characterization and its antimicrobial properties with phytochemicals screening. J Nepal Chem Soc. 2025;45(1):111–21.
[8] Sindhwani S, Chan WC. Nanotechnology for modern medicine: next step towards clinical translation. J Intern Med. 2021;290(3):486–98.
[9] Nelaturi P, Nagarajan P, Sabapathy SK, Sambandam R. Swarna bindu prashana – an ancient approach to improve the infant’s immunity. Biol Trace Elem Res. 2021;199:2145–8.
[10] Kučuk N, Primožič M, Knez Ž, Leitgeb M. Sustainable biodegradable biopolymer-based nanoparticles for healthcare applications. Int J Mol Sci. 2023;24(4):3188.
[11] Muruganandham M, Al-Otibi FO, Alharbi RI, Sivasubramanian K, Chaulagain A, Velmurugan P, et al. Tabebuia rosea seed extract mediated synthesis of silver nanoparticles with antibacterial, antioxidant, and antiproliferative activities. Mater Res Express. 2023;10(12):125006.
[12] Chen J, Zhang X, Millican R, Sherwood J, Martin S, Jo H, et al. Recent advances in nanomaterials for therapy and diagnosis for atherosclerosis. Adv Drug Deliv Rev. 2021;170:142–99.
[13] Aung T, Coleman J, Davidson PW, Hetzel DJ, Aung ST. Intravenous iron infusion and newer non-dextran formulations. Chall COVID-19 Vaccines Prot N Z Popul. 2021;134(1534):118–27.
[14] He Y, Tian F, Zhou J, Zhao Q, Fu R, Jiao B. Colorimetric aptasensor for ochratoxin A detection based on enzyme-induced gold nanoparticle aggregation. J Hazard Mater. 2020;388:121758.
[15] Meng Z, Huang H, Huang D, Zhang F, Mi P. Functional metal–organic framework-based nanocarriers for accurate

magnetic resonance imaging and effective eradication of breast tumor and lung metastasis. J Colloid Interface Sci. 2021;581:31–43.
[16] Khan AU, Khan M, Khan AA, Parveen A, Ansari S, Alam M. Effect of phyto-assisted synthesis of magnesium oxide nanoparticles (MgO-NPs) on bacteria and the root-knot nematode. Bioinorg Chem Appl. 2022;2022:3973841.
[17] Bhardwaj K, Chopra C, Bhardwaj P, Dhanjal DS, Singh R, Najda A, et al. Biogenic metallic nanoparticles from seed extracts: Characteristics, properties, and applications. J Nanomater. 2022;2022:2271278
[18] Sharma SK, Khan AU, Khan M, Gupta M, Gehlot A, Park S, et al. Biosynthesis of MgO nanoparticles using Annona squamosa seeds and its catalytic activity and antibacterial screening. Micro Nano Lett. 2020;15(1):30–4.
[19] Khan M, Khan AU, Moon IS, Felimban R, Alserihi R, Alsanie WF, et al. Synthesis of biogenic silver nanoparticles from the seed coat waste of pistachio (Pistacia vera) and their effect on the growth of eggplant. Nanotechnol Rev. 2021;10(1):1789–800.
[20] Banu R, Bhagavanth Reddy G, Ayodhya D, Ramakrishna D, Kotu GM. Biogenic Pd-nanoparticles from Lantana trifolia seeds extract: Synthesis, characterization, and catalytic reduction of textile dyes. Results Chem. 2023;5:100737.
[21] Khan AU, Khan M, Cho MH, Khan MM. Selected nanotechnologies and nanostructures for drug delivery, nanomedicine and cure. Bioprocess Biosyst Eng. 2020;43(8):1339–57.
[22] Rajkumar G, Sundar R. Biogenic one-step synthesis of silver nanoparticles (AgNPs) using an aqueous extract of Persea americana seed: Characterization, phytochemical screening, antibacterial, antifungal and antioxidant activities. Inorg Chem Commun. 2022;143:109817.
[23] Elangovan U, Anbarasu K, Shanmugam R, Veeramuthu D, John JG. Biological properties of mycosynthesized novel strontium oxide nanoparticles from biomass free filtrate of endophytic fungus Aspergillus sp. LCJ315. BioNanoScience. 2024;14(3):2145–58.
[24] Hughes KJ, Ganesan M, Tenchov R, Iyer KA, Ralhan K, Diaz LL, et al. Nanoscience in action: Unveiling emerging trends in materials and applications. ACS Omega. 2025;10(8):7530–48.
[25] Hussain A, AlAjmi MF, Rehman MT, Amir S, Husain FM, Alsalme A, et al. Copper (II) complexes as potential anticancer and Nonsteroidal anti-inflammatory agents: In vitro and in vivo studies. Sci Rep. 2019;9(1):5237.
[26] Ji P, Wang P, Chen H, Xu Y, Ge J, Tian Z, et al. Potential of copper and copper compounds for anticancer applications. Pharmaceuticals. 2023;16(2):234.
[27] Elango P, Ramar S, Gurusamy A, Muthukutty B, Jeganathan P, Sivakumar M. Bio fabrication of copper oxide nanoparticles using traditional plants, along with their investigation into biological and environmental applications. Colloids Surf A: Physicochem Eng Asp. 2025;709:136147.
[28] Izydorczyk G, Sienkiewicz-Cholewa U, Baśladyńska S, Kocek D, Mironiuk M, Chojnacka K. New environmentally friendly bio-based micronutrient fertilizer by biosorption: From laboratory studies to the field. Sci Total Environ. 2020;710:136061.
[29] Husain N, Mahmood R. Copper (II) generates ROS and RNS, impairs antioxidant system and damages membrane and DNA in human blood cells. Environ Sci Pollut Res. 2019;26:20654–68.
[30] Molinaro C, Martoriati A, Pelinski L, Cailliau K. Copper complexes as anticancer agents targeting topoisomerases I and II. Cancers. 2020;12(10):2863.
[31] Blobaum KJ, Van Heerden D, Wagner AJ, Fairbrother DH, Weihs TP. Sputter-deposition and characterization of paramelaconite. J Mater Res. 2003;18:1535–42.
[32] Zughaibi TA, Jabir NR, Khan AU, Khan MS, Tabrez S. Screening of Cu_4O_3 NPs efficacy and its anticancer potential against cervical cancer. Cell Biochem Funct. 2023;41(8):1174–87.
[33] Yruela I. Copper in plants: acquisition, transport and interactions. Funct Plant Biol. 2009;36(5):409–30.
[34] Manceau A, Nagy KL, Marcus MA, Lanson M, Geoffroy N, Jacquet T, et al. Formation of metallic copper nanoparticles at the soil − root interface. Environ Sci Technol. 2008;42(5):1766–72.
[35] Lava MB, Muddapur UM, Basavegowda N, More SS, More VS. Characterization, anticancer, antibacterial, anti-diabetic and anti-inflammatory activities of green synthesized silver nanoparticles using Justica wynaadensis leaves extract. Mater Today: Proc. 2021;46:5942–7.
[36] Basavegowda N, Somu P, Shabbirahmed AM, Gomez LA, Thathapudi JJ. Bimetallic p-ZnO/n-CuO nanocomposite synthesized using Aegle marmelos leaf extract exhibits excellent visible-light-driven photocatalytic removal of 4-nitroaniline and methyl orange. Photochem Photobiol Sci. 2022;21(8):1357–70.
[37] Mishra K, Basavegowda N, Lee YR. Biosynthesis of Fe, Pd, and Fe–Pd bimetallic nanoparticles and their application as recyclable catalysts for [3 + 2] cycloaddition reaction: a comparative approach. Catal Sci Technol. 2015;5(5):2612–21.
[38] Yang C, Wang B, Wang J, Xia S, Wu Y. Effect of pyrogallic acid (1, 2, 3-benzenetriol) polyphenol-protein covalent conjugation reaction degree on structure and antioxidant properties of pumpkin (Cucurbita sp.) seed protein isolate. Lwt. 2019;109:443–9.
[39] Rezig L, Chouaibi M, Meddeb W, Msaada K, Hamdi S. Chemical composition and bioactive compounds of Cucurbitaceae seeds: Potential sources for new trends of plant oils. Process Saf Environ Prot. 2019;127:73–81.
[40] Meru G, Fu Y, Leyva D, Sarnoski P, Yagiz Y. Phenotypic relationships among oil, protein, fatty acid composition and seed size traits in Cucurbita pepo. Sci Hortic. 2018;233:47–53.
[41] Chari KY, Polu PR, Shenoy RR. An appraisal of pumpkin seed extract in 1, 2-dimethylhydrazine induced colon cancer in wistar rats. J Toxicol. 2018;2018:6086490.
[42] Shandilya U, Sharma A. Functional foods and their benefits: an overview. J Nutr Health Food Eng. 2017;7(4):353–6.
[43] Abou-Zeid SM, AbuBakr HO, Mohamed MA, El-Bahrawy A. Ameliorative effect of pumpkin seed oil against emamectin induced toxicity in mice. Biomed Pharmacother. 2018;98:242–51.
[44] Aktaş N, Uzlaşır T, Tunçil YE. Pre-roasting treatments significantly impact thermal and kinetic characteristics of pumpkin seed oil. Thermochim Acta. 2018;669:109–15.
[45] Amin MZ, Islam T, Uddin MR, Uddin MJ, Rahman MM, Satter MA. Comparative study on nutrient contents in the different parts of indigenous and hybrid varieties of pumpkin (Cucurbita maxima Linn.). Heliyon. 2019;5(9):02462.
[46] Aziz AR, AbouLaila MR, Aziz M, Omar MA, Sultan K. In vitro and in vivo anthelmintic activity of pumpkin seeds and pomegranate peels extracts against Ascaridia galli. Beni-Suef Univ J Basic Appl Sci. 2018;7(2):231–4.
[47] Jafari M, Goli SAH, Rahimmalek M. The chemical composition of the seeds of Iranian pumpkin cultivars and physicochemical characteristics of the oil extract. Eur J Lipid Sci Technol. 2012;114(2):161–7.

[48] Naziri E, Mitić MN, Tsimidou MZ. Contribution of tocopherols and squalene to the oxidative stability of cold-pressed pumkin seed oil (Cucurbita pepo L.). Eur J Lipid Sci Technol. 2016;118(6):898–905.
[49] Dakeng S, Duangmano S, Jiratchariyakul W, U-Pratya Y, Bögler O, Patmasiriwat P. Inhibition of Wnt signaling by cucurbitacin B in breast cancer cells: Reduction of Wnt-associated proteins and reduced translocation of galectin-3-mediated β-catenin to the nucleus. J Cell Biochem. 2012;113(1):49–60.
[50] Aghaei S, Nikzad H, Taghizadeh M, Tameh AA, Taherian A, Moravveji A. Protective effect of Pumpkin seed extract on sperm characteristics, biochemical parameters and epididymal histology in adult male rats treated with Cyclophosphamide. Andrologia. 2014;46(8):927–35.
[51] Chonoko U, Rufai A. Phytochemical screening and antibacterial activity of Cucurbita pepo (Pumpkin) against Staphylococcus aureus and Salmonella typhi. Bayero J Pure Appl Sci. 2011;4(1):145–7.
[52] Jayaprakasam B, Seeram NP, Nair MG. Anticancer and antiinflammatory activities of cucurbitacins from Cucurbita andreana. Cancer Lett. 2003;189(1):11–6.
[53] Brogan DM, Mossialos E. A critical analysis of the review on antimicrobial resistance report and the infectious disease financing facility. Global Health. 2016;12:1–7.
[54] Abd El-Aziz A, Abd El-Kalek H. Antimicrobial proteins and oil seeds from pumpkin (Cucurbita moschata). Nat Sci. 2011;9(3):105–19.
[55] Kabbashi AS, Koko WS, Mohammed SE, Musa N, Osman EE, Dahab MM, et al. In vitro amoebicidal, antimicrobial and antioxidant activities of the plants Adansonia digitata and Cucurbit maxima. Adv Med Plant Res. 2014;2(3):50–7.
[56] Bharti SK, Kumar A, Sharma NK, Prakash O, Jaiswal SK, Krishnan S, et al. Tocopherol from seeds of Cucurbita pepo against diabetes: Validation by in vivo experiments supported by computational docking. J Formos Med Assoc. 2013;112(11):676–90.
[57] Alhakamy NA, Fahmy UA, Ahmed OA. Attenuation of benign prostatic hyperplasia by optimized tadalafil loaded pumpkin seed oil-based self nanoemulsion: *In vitro* and *in vivo* evaluation (Retraction of Vol 11, art no 640, 2019). ST ALBAN-ANLAGE 66, CH-4052 BASEL, SWITZERLAND: MDPI; 2023.
[58] Gossell-Williams M, Davis A, O'connor N. Inhibition of testosterone-induced hyperplasia of the prostate of sprague-dawley rats by pumpkin seed oil. J Med Food. 2006;9(2):284–6.
[59] Ren S, Ouyang D-Y, Saltis M, Xu LH, Zha QB, Cai JY, et al. Anti-proliferative effect of 23, 24-dihydrocucurbitacin F on human prostate cancer cells through induction of actin aggregation and cofilin-actin rod formation. Cancer Chemother Pharmacol. 2012;70:415–24.
[60] Dhariwala MY, Ravikumar P. An overview of herbal alternatives in androgenetic alopecia. J Cosmet Dermatol. 2019;18(4):966–75.
[61] Hajhashemi V, Rajabi P, Mardani M. Beneficial effects of pumpkin seed oil as a topical hair growth promoting agent in a mice model. Avicenna J Phytomed. 2019;9(6):499–504.
[62] Alhawiti AO, Toulah FH, Wakid MH. Anthelmintic potential of Cucurbita pepo Seeds on Hymenolepis nana. Acta Parasitol. 2019;64:276–81.
[63] Ezea BO, Ogbole OO, Ajaiyeoba EO. In vitro anthelmintic properties of root extracts of three Musa species. J Pharm Bioresour. 2019;16(2):145–51.
[64] Balbino S, Dorić M, Vidaković S, Kraljić K, Škevin D, Drakula S, et al. Application of cryogenic grinding pretreatment to enhance extractability of bioactive molecules from pumpkin seed cake. J Food Process Eng. 2019;42(8):e13300.
[65] Fruhwirth GO, Wenzl T, El-Toukhy R, Wagner FS, Hermetter A. Fluorescence screening of antioxidant capacity in pumpkin seed oils and other natural oils. Eur J Lipid Sci Technol. 2003;105(6):266–74.
[66] Zhang L, Fan X-R, Xie H, He QH, Nie YS, Zhang M, et al. Anti-Inflammatory and antioxidant effects of kelong-capsule on testosterone-induced benign prostatic hyperplasia in rats. Evid-Based Complemen Altern Med. 2018;2018:5290514.
[67] Das G, Patra JK, Basavegowda N, Vishnuprasad CN, Shin HS. Comparative study on antidiabetic, cytotoxicity, antioxidant and antibacterial properties of biosynthesized silver nanoparticles using outer peels of two varieties of Ipomoea batatas (L.) Lam. Int J Nanomed. 2019;14:4741–54.
[68] Thanuja J, Nagaraju G, Naika H. Biosynthesis of Cu_4O_3 nanoparticles using Razma seeds: application to antibacterial and cytotoxicity activities. SN Appl Sci. 2019;1(12):1646.
[69] Ibrahim S, Ahmad Z, Manzoor MZ, Mujahid M, Faheem Z, Adnan A. Optimization for biogenic microbial synthesis of silver nanoparticles through response surface methodology, characterization, their antimicrobial, antioxidant, and catalytic potential. Sci Rep. 2021;11(1):770.
[70] Goemaere I, Punj D, Harizaj A, Woolston J, Thys S, Sterck K, et al. Response surface methodology to efficiently optimize intracellular delivery by photoporation. Int J Mol Sci. 2023;24(4):3147.
[71] Abu-Elghait M, Soliman MK, Azab MS, Salem SS. Response surface methodology: Optimization of myco-synthesized gold and silver nanoparticles by Trichoderma saturnisporum. Biomass Convers Biorefin. 2025;15(3):4211–24.
[72] Nachiyar GKV, Surendra TV, Kalaiselvi V, Rajagopal R, Kuppusamy P, Basavegowda N, et al. Box–Behnken response surface methodology design for amaranth dye degradation using gold nanoparticles. Optik. 2022;267:169633.
[73] Ferreira SL, Bruns RE, Ferreira HS, Matos GD, David JM, Brandão GC, et al. Box-Behnken design: an alternative for the optimization of analytical methods. Anal Chim Acta. 2007;597(2):179–86.
[74] Minitab®. Minitab LLC 2022; 22.2.2.0. Available from: https://www.minitab.com/.
[75] Ghasemi M, Turnbull T, Sebastian S, Kempson I. The MTT assay: utility, limitations, pitfalls, and interpretation in bulk and single-cell analysis. Int J Mol Sci. 2021;22(23):12827.
[76] Frisch M. Gaussian 03 rev. E. 01; 2004. http://www.gaussian.com/.
[77] Tabrez S, Khan AU, Hoque M, Suhail M, Khan MI, Zughaibi TA. Investigating the anticancer efficacy of biogenic synthesized MgONPs: An in vitro analysis. Front Chem. 2022;10:970193.
[78] Hagos M, Redi-Abshiro M, Chandravanshi BS, Yaya EE. Development of analytical methods for determination of β-carotene in pumpkin (Cucurbita maxima) flesh, peel, and seed powder samples. Int J Anal Chem. 2022;2022(1):9363692.
[79] Khorsand Zak A, Mahmoudian M, Darroudi M, Yousefi R. Starch-stabilized synthesis of ZnO nanopowders at low temperature and optical properties study. Adv Powder Technol. 2013;24(3):618–24.
[80] Halim NRA, Azlan A, Yusof HM, Sarbon NM. Antioxidant and anticancer activities of enzymatic eel (Monopterus sp) protein hydrolysate as influenced by different molecular weight. Biocatal Agric Biotechnol. 2018;16:10–6.

[81] Li Y, Chen M, Khan AH, Ma Y, He X, Yang J, et al. Temperature-modulated solution-based synthesis of copper oxide nanostructures for glucose sensing. Mater Adv. 2023;4(16):3572–82.
[82] Dwivedi P, Malik A, Fatima Hussain HZ, Jatrana I, Imtiyaz K, Rizvi M, et al. Eco-friendly CuO/Fe_3O_4 nanocomposite synthesis, characterization, and cytotoxicity study. Heliyon. 2024;10(6):27787.
[83] Jabir NR, Mahboob A, Suhail M, Khan MS, Arshad M, Tabrez S. Anticancer potential of Cu_4O_3 NPs against human ovarian teratocarcinoma: an in-vitro validation. Chem Pap. 2024;78(5):2811–21.
[84] Wongrakpanich A, Mudunkotuwa IA, Geary SM, Morris AS, Mapuskar KA, Spitz DR, et al. Size-dependent cytotoxicity of copper oxide nanoparticles in lung epithelial cells. Environ Sci: Nano. 2016;3(2):365–74.
[85] City S, Sugata M, Jan T, editors. Probiotic characterization of Bacillus subtilis SM10. 1. Journal of Physics: Conference Series. IOP Publishing; 2021.
[86] Madiha BSK, Zahid Q, Ali H. Biogenically fabricated TMO-NPs and their anti-bacterial and fungal assay (well diffusion method) in saline solution. Nanomed Nanotechnol Open Access. 2020;5(1):000176.
[87] Tarangini K, Sherlin SN, Jakkala S, Borah P, Wacławek S, Sabarinath S, et al. Optimising biosynthesis of antimicrobial copper nanoparticles using aqueous Aegle marmelos leaf extract-based medium. Ecol Chem Eng. 2024;31(1):7–17.
[88] Thandapani G, Arthi K, Pazhanisamy P, John JJ, Vinothini C, Rekha V, et al. Green synthesis of copper oxide nanoparticles using Spinacia oleracea leaf extract and evaluation of biological applications: Antioxidant, antibacterial, larvicidal and biosafety assay. Mater Today Commun. 2023;34:105248.